Simulation of Direct Voltage Control for a Stand-Alone Wind-Driven Self-Excited Induction Generator with Improved Power Quality

Satish Kurre*, Ms. Durga Sharma (Assistant Professor) **
*(Department of Electrical and Electronics Engineering, Dr. C.V. Raman University, Bilaspur (C.G.)
** (Department of Electrical and Electronics Engineering, Dr. C.V. Raman University, Bilaspur (C.G.)

Abstract

Control of terminal voltage and frequency of a stand-alone wind-driven self-excited induction generator with variable loads is proposed using an improved direct voltage control (DVC) strategy.

The DVC strategy, including a proportional-integral (PI) regulator, lead–lag corrector, and a feed-forward compensator, is designed based on the system transfer function matrix. The PI regulator can eliminate the steady-state tracking errors of the terminal voltage. The lead–lag corrector is employed to enlarge the phase stability margin of the dominant loops while the feedforward compensator is adopted to mitigate the voltage harmonics resulting from the cross-coupling dynamics. The simulation and experimental results verify that the proposed strategy has a fast dynamic response and can effectively control the generated voltage with low harmonic distortions under different linear or nonlinear loads.

Index Terms—Direct voltage control (DVC), harmonic compensation, induction generator, stand-alone wind energy conversion systems.

I. INTRODUCTION

STAND-ALONE power systems using local renewable energy sources like wind, biomass, and hydro are attractive to the remote communities [1]. Compared with grid connected counterparts, they avoid long transmission lines and thereby associate losses and cost. The self-excited induction generator (SEIG) is very suitable for such small or medium power systems compared with other generator structures, such as the doubly fed induction generator, because of its low cost, robustness, less maintenance, and inherent overload protection [2]–[4]. However, the magnitude and frequency of the generated voltage depend on the rotor speed, excitation current, and the load. SEIG driven by constant speed prime movers such as biogas and diesel engines has a fixed rotor speed. The frequency variation of the generator terminal voltage is negligible. In order to maintain the voltage magnitude under variable consumer loads, reactive power compensators such as static VAR compensator

or static compensator are necessary [5], [6]. In the application of SEIG with constant power prime movers like micro and hydro turbines, the magnitude and frequency of the generated voltage are varying with different load conditions. In previous research, electronic load controllers (ELCs) have been proposed to balance the generator output power to control the generator voltage [1], [7], [8]. However, since the active power is controlled with a variable ac/dc load in the ELC, the system efficiency is low [9]. For the wind-driven SEIG where wind speed and consumer loads are variable, both input power and rotor speed are not constant which in turn varies the magnitude and frequency of the generated voltage [6], [10]. In such a case, a shunt-connected voltage source inverter (VSI) with an energy storage unit on the dc side, typically a battery bank, can be utilized to absorb or compensate the active and reactive power produced by SEIG. As a result, the magnitude and frequency of the generator voltage can be maintained [3], [6], [9], [10]. Strategies with double control loops were proposed in [6] and [10] for the SEIG–VSI system. The outer frequency and voltage loops determine the references of active and reactive power (or current components) for the inner current loops which then yield the voltage commands for the VSI. Proportional-integral (PI) regulators are normally employed in both control loops to eliminate the steady-state tracking errors. In [9] and [11], direct voltage control (DVC) strategies were presented to control the SEIG–VSI system. With only a single voltage loop, DVC directly controls the voltage magnitude with PI regulators and the frequency with an open-loop phase angle generator. DVC has been validated to have a fast dynamic response with simulation and experimental results [9], [11]. However, the nonlinear load situation is not considered in the present strategy.

In this paper, an improved DVC strategy for the wind-driven SEIG–VSI system is proposed. The procedures for capacity matching of the excitation capacitors, the VSI, and the consumer load are presented. For the resistive load, it is generally hard to reduce the VSI capacity because it has to support the resistive load at low wind speeds. For the inductive load, more excitation capacitors can help to reduce the VSI capacity due to its ability of reactive power supply. The DVC strategy is designed based

on the transfer function matrix of the SEIG–VSI system. It is noticed that the diagonal dominant loops have a narrow phase stability margin in the conventional DVC. Furthermore, the cross-coupling loops have significant effects on the dominant loops in 150–400 Hz frequency bands, which leads to voltage harmonics under nonlinear load conditions. A lead–lag
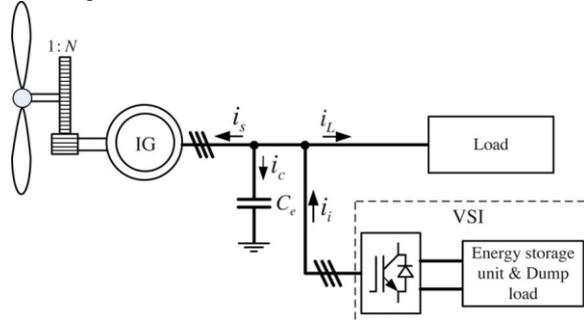
Fig. 1. Block diagram of the SEIG–VSI system.

phase corrector is employed to enlarge the phase stability margin of the dominant loops and a feed-forward compensator loop is proposed to suppress the harmonics due to cross-coupling. The simulation and experimental results verify that the proposed strategy has a fast dynamic response and can effectively suppress the harmonic voltages under various load conditions.

II.   SYSTEM CONFIGURATION AND MODELS

Fig. 1 shows the block diagram of the SEIG–VSI system. The wind turbine is connected to the rotor of the induction generator through a step-up gear box. At the stator side of the generator, there is an excitation capacitor bank in parallel with the VSI and the consumer load. The VSI has an energy storage device, which can be battery or supercapacitor, connected at its dc bus and offers variable controlled impedance across the SEIG terminals to retain the terminal voltage.

A. Modeling of the Wind Turbine
The mechanical power available in a fix-pitch wind turbine, neglecting the losses in the gear box, is given by

$$P_{wt} = 0.5\rho\pi R^2 C_p(\lambda)V^3 \qquad (1)$$

where

ρ air density (kg/m^3);
R radius of the wind turbine (m);
C_p power coefficient of the wind turbine;
v wind speed (m/s);
λ tip speed ratio.

where
ρ air density (kg/m3);
R radius of the wind turbine (m);
C_p power coefficient of the wind turbine;

v wind speed (m/s);
λ tip speed ratio.
The power coefficientC_p varies nonlinearly with the tip speed ratio λ which is defined as the ratio of the turbine rotational speed and the wind speed. A typical C_p versus λ curve for a threeblade wind turbine is shown in Fig. 2 and the detailed equation is described in [12]. It shows that C_p has a unique maximal value in which point the turbine can yield the maximal wind power.

B. Modeling of the SEIG
The model of the induction generator can be developed in the synchronous reference (d–q) frame as follows [2], [13]:

$$v_{ds} = R_s i_{ds} + \frac{d\psi_{ds}}{dt} - \omega_e \psi_{qs}$$

$$v_{qs} = R_s i_{qs} + \frac{d\psi_{qs}}{dt} + \omega_e \psi_{ds}$$
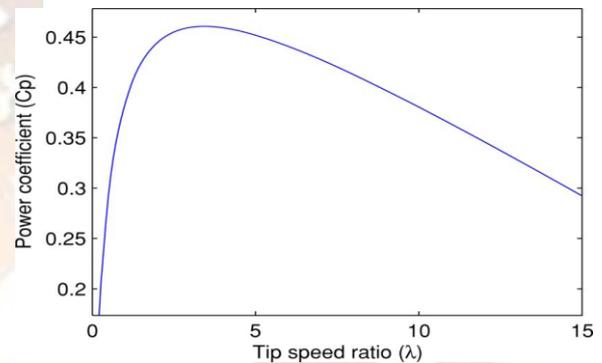
Fig. 2. Typical C_p versus λ curve.

$$v_{dr} = R_r i_{dr} + \frac{d\psi_{dr}}{dt} - (\omega_e - \omega_r)\psi_{qr}$$

$$v_{qr} = R_r i_{qr} + \frac{d\psi_{qr}}{dt} + (\omega_e - \omega_r)\psi_{dr}. \qquad (2)$$

The stator and rotor flux can be computed as functions of the d-and q-axes stator and rotor currents as follows:
$\psi ds = Lls\ ids + Lm(ids + idr)$
$\psi qs = Lls\ iqs + Lm(iqs + iqr)$
$\psi dr = Llr\ idr + Lm(idr + ids)$
$\psi qr = Llr\ iqr + Lm(iqr + iqs).$ (3)

The SEIG excitation capacitors introduce the following state equations in the d–q frame:

$$i_{dc} = C_e \frac{dv_{ds}}{dt} - \omega_e C_e v_{qs}$$

$$i_{qc} = C_e \frac{dv_{qs}}{dt} + \omega_e C_e v_{ds} \qquad (4)$$

where

subscripts *d* and *q* direct and quadrature axes;
subscripts *s* and *r* stator and rotor variables;
subscripts *l* and *m* leakage and mutual components;
subscript *c* excitation variables;
v and *i* instantaneous voltage and current;
L inductance;
R resistance;
Ce excitation capacitance;
ωe synchronous rotational speed;
ωr electrical rotor speed.
It should be noted that the mutual inductance *Lm* is not a constant and it depends on the nonlinear magnetization characteristics of the SEIG [9], [10].

C. Modeling of the VSI and Consumer Load

For the high-frequency switching converters, it is reasonable to describe the converter dynamics with its state-space averaged model [14]. In view of this, the VSI model can be expressed in
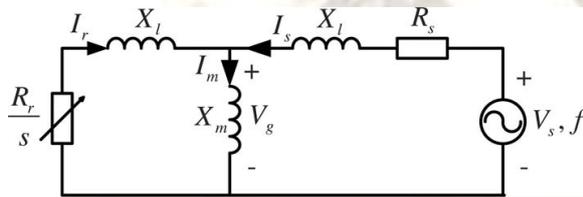
Fig. 3. Single-phase equivalent circuit of the SEIG–VSI system

the *d–q* frame as follows:

$$v_{ds} = v_{di} - L\frac{di_{di}}{dt} + \omega_e L i_{qi}$$

$$v_{qs} = v_{qi} - L\frac{di_{qi}}{dt} - \omega_e L i_{di} \qquad (5)$$

where the subscript *i* represents the VSI variables and *L* is the filter inductance. The model of a typical *R–L* load can be represented in the *d–q* frame as follows:

$$v_{ds} = R_L i_{dL} + L_L\frac{di_{dL}}{dt} - \omega_e L_L i_{qL}$$

$$v_{qs} = R_L i_{qL} + L_L\frac{di_{qL}}{dt} + \omega_e L_L i_{dL} \qquad (6)$$

where the subscript *L* represents the load variables. In the same reference frame, the currents of the SEIG–VSI system shown in Fig. 1 are related by
idi = ids + idc + idL
iqi = iqs + iqc + iqL
(7)

where the subscript *c* represents the excitation capacitor variables.

III.   STEADY-STATE ANALYSIS

Fig. 3 shows the per-unit per-phase steady-state equivalent circuit of the SEIG–VSI system. The VSI, excitation capacitors, and the consumer load are represented by an ideal voltage source *Vs* since the generator terminal voltage is kept constant in steady state. It is assumed that the harmonics of the voltage and current at switching frequency are negligible. The rotor and stator resistances of the induction generator are referred to the stator side and the leakage inductances of the rotor and stator are assumed to be equal in magnitude (*Xlr = Xls = Xl*). All machine parameters are assumed to be constant except the magnetizing reactance *Xm* and the slip frequency *s*. The nonlinear magnetization curve at base frequency is approximated with a piecewise function as listed in Appendix I.

A. Output Power of the Induction Generator Under Different Wind Speeds

In the steady state, the mechanical power introduced to the induction generator can be expressed with the slip frequency *s*, rotor current *Ir* , and resistance *Rr* as [13] follows:

$$P_{\text{in}} = -3\frac{1-s}{s}I_r^2 R_r. \qquad (8)$$
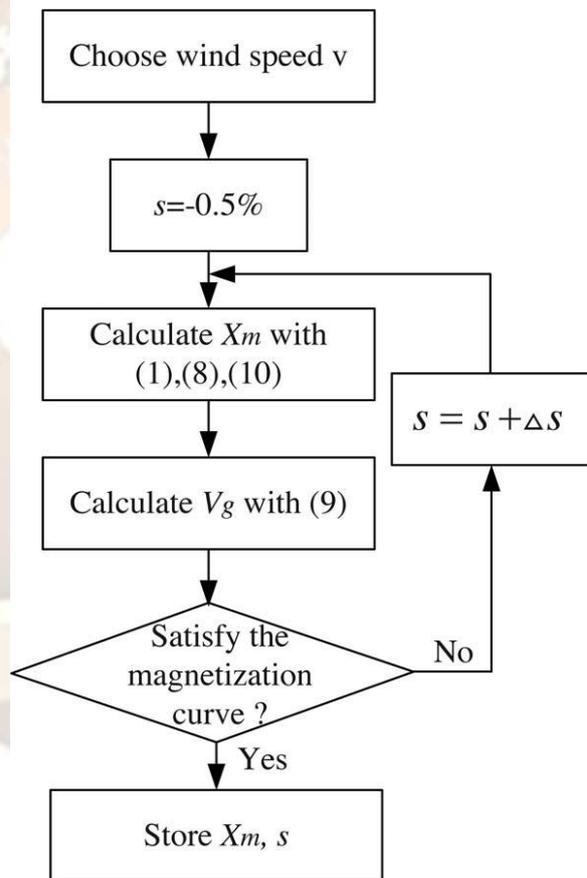
Fig. 4. Flow chart of the incremental search algorithm..

Applying Kirchhoff laws to the circuit in Fig. 3, we have

$$I_r = -\frac{V_g}{Z_r}$$

$$I_s = \frac{V_g}{Z_1} = \frac{V_s}{Z_2} \qquad (9)$$

where

$$Z_r = \sqrt{(R_r/s)^2 + X_l^2}; \qquad Z_1 = \sqrt{A^2 + B^2}$$

$$Z_2 = \sqrt{(A + R_s)^2 + (B + X_l)^2}$$

$$A = \frac{R_r X_m^2/s}{(R_r/s)^2 + (X_l + X_m)^2}$$

$$B = \frac{(R_r/s)^2 X_m + X_l X_m (X_l + X_m)}{(R_r/s)^2 + (X_l + X_m)^2}.$$

Ignoring the losses of the shaft and gear box, the input mechanical power Pin equals to the wind power extracted by the wind turbine
Pin = Pwt. (10)

An incremental search algorithm [10], [15] was implemented to solve the steady-state operation points of the SEIG–VSI system with (1), (8), (9), and (10). The flow chart of the search algorithm can be illustrated in Fig. 4. The calculation starts with the rated wind speed (9 m/s) and the same procedure is repeated at other wind speeds. Based on the solutions of Xm and s at different wind speeds, the active/reactive power produced/consumed by the generator is obtained. The generator produces more active power and consumes more reactive power with a higher wind speed.

Compared with the active power variation, the reactive power varies in a relatively narrow interval (from 1.07 to 1.25 pu) within the available wind speed range. The rated active power of the induction generator is selected as the base value.

B. Capacity Matching of the VSI, Excitation Capacitors, and Consumer Load

In Fig. 3, the power produced by the generator should equal to the power flowing into the equivalent voltage source Vs due to the power balance. Since Vs represents the VSI, excitation capacitors, and the consumer load, following power equations hold true:
PIG = PVSI − PL
QIG = QVSI + QC − QL . (11)

Since the presented system is a fixed-speed wind energy conversion system (WECS), the active and reactive power of the SEIG can be related to the wind speed.
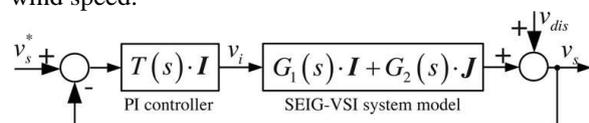
Fig. 7. Control diagram of the SEIG–VSI system with conventional DVC. so that a wide operation

range can be guaranteed. Moreover, the average local wind speed can be further utilized to optimize the system capacities.

IV.   IMPROVED DVC

The control objective of the VSI is to maintain the terminal voltage of SEIG even with variable wind speeds or consumer loads. In view of this, the system control inputs are selected as the VSI voltage *vdi, vqi* and the outputs are the generator terminal voltage *vds, vqs*. From (2) to (7), the I/O transfer function matrix of the SEIG– VSI system is as follows:

$$v_s(s) = [G_1(s) \cdot \mathbf{I} + G_2(s) \cdot \mathbf{J}] v_i(s) \qquad (12)$$

where

$$v_s(s) = [v_{ds}(s) \quad v_{qs}(s)]^T \quad v_i(s) = [v_{di}(s) \quad v_{qi}(s)]^T$$

$$\mathbf{I} = \begin{bmatrix} 1 & 0 \\ 0 & 1 \end{bmatrix} \quad \mathbf{J} = \begin{bmatrix} 0 & -1 \\ 1 & 0 \end{bmatrix}$$

$G1$ (s) and $G2$ (s) are the dominant and cross-coupling transfer functions of the I/O and they are listed in Appendix II. Here, the magnetizing saturation is not concerned because the generator should be designed to operate in the linear parts of the magnetization curve in the desired wind speed range in order to obtain a satisfactory performance. Thus, Lm is considered as a constant in this section. For such a multiinput multioutput (MIMO) system, a popular technique in the industry is to follow the control design procedures for single-input single-output (SISO) systems, in which the cross-coupling items are considered as disturbances. Motivations comes from the fact that many systems can be made diagonally dominant (i.e., interactions between loops are not predominant) by designing appropriated decoupling decompensators
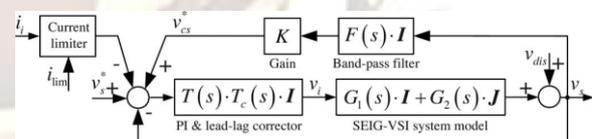
Fig. 9. Control diagram of the SEIG–VSI system with improved DVC.

[16]. The PI controller can be applied to the dominant
loops [9] resulting in the control diagram as depicted in Fig. 7, where $T(s) = kp + ki/s$ and *v*dis represents the disturbances caused by the load variations.
The open-loop transfer function matrix of the whole system shown in Fig. 7 is

$$G(s) = T(s)[G_1(s) \cdot \mathbf{I} + G_2(s) \cdot \mathbf{J}]. \qquad (13)$$

Usually, the generator speed responses much slower than the electrical variables due to the large turbine and generator inertias. And the operating slip frequency of the wind-driven SEIG shown in Fig. 1 is

around −5 to −1%, which has negligible effects on the system characteristics.

V.   SIMULATION RESULTS
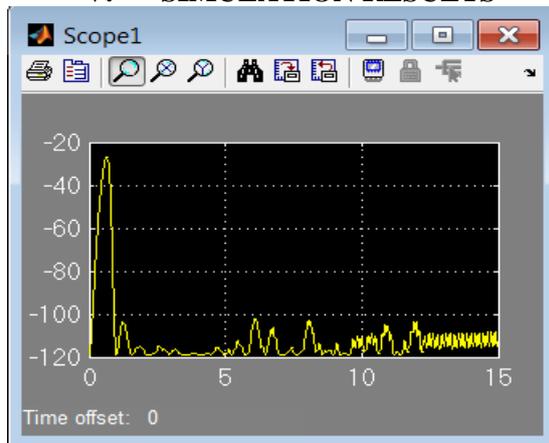
Tm
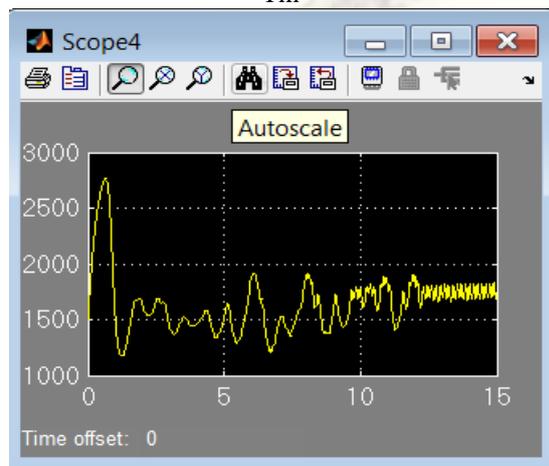
Rotor Speed
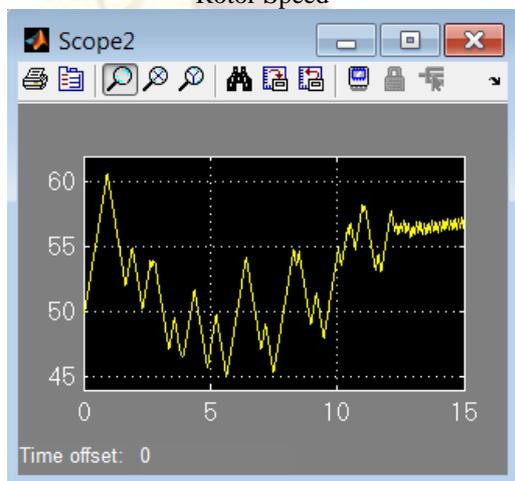
Frequency
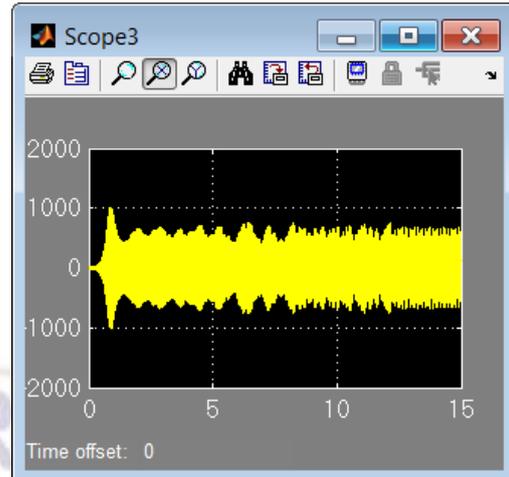
Phase A Voltage
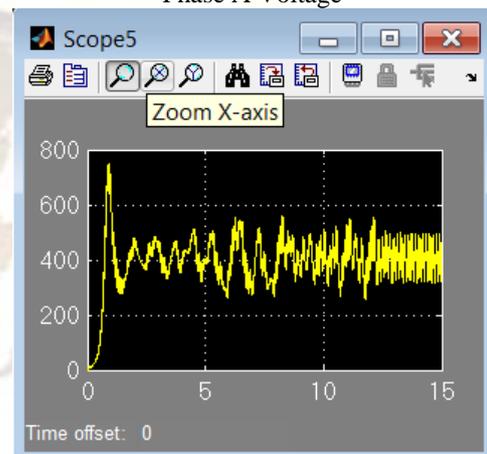
RMS Value of Phase A Voltage
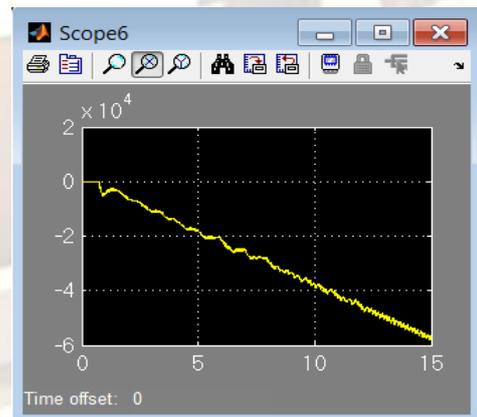
OUTPUT OF PID CONTROLLER

VI.   CONCLUSION

This paper has presented the procedures for the capacity and controller design of the stand-alone wind-driven SEIG–VSI system. The VSI capacity can be optimized following the capacity matching calculations for a given load range. For the inductive load, more excitation capacitors can help to reduce the VSI capacity because its ability of reactive power supply. In the industry, the conventional technique for the controller design of a MIMO system such as

the SEIG–VSI is to follow the procedures for SISO systems, in which the cross-coupling loops are considered as disturbances or compensated with decoupling items. However, as shown in this paper, it is difficult to execute the decoupling compensations for the SEIG–VSI system since the system parameters are normally unknown. Moreover, the influences of the coupling dynamics cannot be ignored in some frequency bands. In such a case, the compensation can be implemented in the diagonal dominant loops, which provides active damping on the effects of coupling dynamics.

REFERENCES

[1] B. Singh, S. Murthy, and S. Gupta, "Transient analysis of self-excited induction generator with electronic load controller (ELC) supplying static and dynamic loads," *IEEE Trans. Ind. Appl.*, vol. 41, no. 5, pp. 1194–1204, Sep./Oct. 2005.

[2] M. G. Simoes and F. A. Farret, *Alternative Energy Systems: Design and Analysis With Induction Generators*, 2nd ed. Boca Raton, FL: CRC Press, 2007.

[3] J. Chatterjee, B. Perumal, and N. Gopu, "Analysis of operation of a selfexcited induction generatorwith generalized impedance controller," *IEEE Trans. Energy Convers.*, vol. 22, no. 2, pp. 307–315, Jun. 2007.

[4] K. Protsenko and D. Xu, "Modeling and control of brushless doubly-fed induction generators in wind energy applications," *IEEE Trans. Power Electron.*, vol. 23, no. 3, pp. 1191–1197, May 2008.

[5] B. Singh, S. Murthy, and S. Gupta, "Analysis and design of statcom-based voltage regulator for self-excited induction generators," *IEEE Trans. Energy Convers.*, vol. 19, no. 4, pp. 783–790, Dec. 2004.

[6] B. Singh and G. Kasal, "Solid state voltage and frequency controller for a stand alone wind power generating system," *IEEE Trans. Power Electron.*, vol. 23, no. 3, pp. 1170–1177, May 2008.

[7] B. Singh, S. Murthy, and S. Gupta, "Analysis and design of electronic load controller for self-excited induction generators," *IEEE Trans. Energy Convers.*, vol. 21, no. 1, pp. 285–293, Mar. 2006.

[8] J. M. Ramirez and M. E. Torres, "An electronic load controller for the self-excited induction generator," *IEEE Trans. Energy Convers.*, vol. 22, no. 2, pp. 546–548, Jun. 2007.

[9] B. Venkatesa Perumal and J. Chatterjee, "Voltage and frequency control of a stand alone brushless wind electric generation using generalized impedance controller,"

IEEE Trans. Energy Convers., vol. 23, no. 2, pp. 632–641, Jun. 2008.

[10] L. Lopes and R. Almeida, "Wind-driven self-excited induction generator with voltage and frequency regulated by a reduced-rating voltage source inverter," *IEEE Trans. Energy Convers.*, vol. 21, no. 2, pp. 297–304, Jun. 2006.

[11] W. Huang and D. Xu, "Direct voltage control for standalone wind energy conversion systems with induction generator and energy storage," in *Proc. IEEE Electric Power Conf.(EPEC)*, Oct. 2008, pp. 1–8.

[12] G. Stavrakakis and G. Kariniotakis, "A general simulation algorithm for the accurate assessment of isolated diesel-wind turbines systems interaction. i. a general multimachine power system model," *IEEE Trans. Energy Convers.*, vol. 10, no. 3, pp. 577–583, Sep. 1995.

[13] B. K. Bose, *Modern Power Electronics and AC Drives*. Upper Saddle River, NJ: Prentice Hall, 2002.

[14] D. Maksimovic, A. Stankovic, V. Thottuvelil, and G. Verghese, "Modeling and simulation of power electronic converters," *Proc. IEEE*, vol. 89, no. 6, pp. 898–912, Jun. 2001.

[15] S. Singh, B. Singh, andM. Jain, "Performance characteristics and optimum utilization of a cage machine as capacitance excited induction generator," *IEEE Trans. Energy Convers.*, vol. 5, no. 4, pp. 679–685, Dec. 1990.

[16] D. Chen and D. Seborg, "Multiloop PI/PID controller design based on gershgorin bands," *IEE Proc. Control Theory Appl.*, vol. 149, no. 1, pp. 68–73, Jan. 2002.

[17] R. Teodorescu and F. Blaabjerg, "Flexible control of small wind turbines with grid failure detection operating in stand-alone and grid-connected mode," *IEEE Trans. Power Electron.*, vol. 19, no. 5, pp. 1323–1332, Sep. 2004.